

Cite this: *RSC Adv.*, 2017, 7, 38452

# Low-cost solution-processed digenite $\text{Cu}_9\text{S}_5$ counter electrode for dye-sensitized solar cells†

Maowei Hu,<sup>a</sup> Ze Yu,<sup>ID</sup> <sup>\*a</sup> JiaJia Li,<sup>a</sup> Xiaoqing Jiang,<sup>a</sup> Jianbo Lai,<sup>a</sup> Xichuan Yang,<sup>ID</sup> <sup>a</sup> Mei Wang,<sup>ID</sup> <sup>\*a</sup> and Licheng Sun,<sup>ID</sup> <sup>ab</sup>

The development of low-cost alternatives to the commonly used but expensive platinum (Pt) catalyst in dye-sensitized solar cells (DSSCs) is important from a commercial point of view. In this work,  $\text{Cu}_9\text{S}_5$  nanocrystalline film is fabricated directly onto a F-doped  $\text{SnO}_2$  (FTO) substrate by a solution-processed spin-coating method with low temperature post-treatment at 250 °C and it is further explored as a counter electrode (CE) material in DSSCs. The results from cyclic voltammetry (CV) and electrochemical impedance spectroscopy (EIS) disclose that  $\text{Cu}_9\text{S}_5$  film exhibits a higher catalytic ability for the state-of-the-art cobalt(II/III) tris(bipyridyl) ( $[\text{Co}(\text{bpy})_3]^{2+/3+}$ ) redox system as compared to the widely used iodine-based electrolyte. Consequently, the DSSC devices based on the cobalt complex redox shuttles show a power conversion efficiency (PCE) of 5.7% measured at 100  $\text{mW cm}^{-2}$  illumination (AM 1.5G), which is substantially higher than that of the iodine-based counterpart (3.9%). This has been the first presentation for the application of digenite copper sulfides as an electrocatalyst for the  $[\text{Co}(\text{bpy})_3]^{2+/3+}$  redox system in DSSCs. The present finding represents a promising solution for the development of alternative cost-effective CE materials for DSSCs in the future.

Received 19th June 2017

Accepted 31st July 2017

DOI: 10.1039/c7ra06822k

rsc.li/rsc-advances

## 1. Introduction

Dye-sensitized solar cells (DSSCs) have been widely studied as promising next-generation solar cells since 1991, owing to their low production cost, ease of manufacture, and comparatively high PCE.<sup>1</sup> A DSSC device typically consists of three major parts: a mesoporous  $\text{TiO}_2$  photoanode loaded with a dye molecule, a liquid electrolyte typically involving an iodide/triiodide ( $\text{I}^-/\text{I}_3^-$ ) redox couple and a CE. After light absorption, the oxidized dye transfers electrons into the  $\text{TiO}_2$  semiconductor. The dye molecule cations are then regenerated by iodide, while the CE reduces the triiodide back to iodide at the CE/electrolyte interface.

Through intense investigations over the past twenty years, remarkable improvements have been achieved in the research field of DSSCs. A big breakthrough was made by replacing the  $\text{I}^-/\text{I}_3^-$  redox system with a  $[\text{Co}(\text{bpy})_3]^{2+/3+}$  redox couple, which possesses a more positive redox potential, thus giving a much higher open-circuit voltage ( $V_{\text{oc}}$ ) and higher PCEs.<sup>2,3</sup> The highest PCE of DSSCs has reached ~13% by using  $[\text{Co}(\text{bpy})_3]^{2+/3+}$  system in combination with panchromatic co-photosensitizers.<sup>4</sup>

CE acts as a catalyst for the regeneration of the redox couple, which is an indispensable part in DSSCs and is the key for determining the overall performance.<sup>5</sup> Noble metal Pt was extensively applied as CE catalyst material since the very beginning of DSSC research, because of the excellent catalytic ability for the  $\text{I}_3^-$  reduction and good electrical conductivity. Nevertheless, Pt is rarely reserved in the earth and the fabrication process typically involves high temperature, which limit its large-scale application in the future. Searching for a low-cost alternative CE catalyst is therefore absolutely necessary.

To replace Pt CE, a number of alternative materials has been studied, for instance, carbon-based materials,<sup>6</sup> conducting polymers<sup>7</sup> as well as metal complexes.<sup>8</sup> Metal sulfides, such as  $\text{CoS}$ ,  $\text{NiS}$ ,  $\text{FeS}_2$ ,  $\text{WS}_2$ , and  $\text{MoS}_2$ , have also been developed as alternative CEs, showing comparable or even higher PCEs relative to the Pt-based counterparts.<sup>9–17</sup> Among the family of metal sulfides, several copper sulfide compounds, which showed good catalytic property, high conductivity, as well as economical fabrication, have attracted much attention in quantum dot-sensitized solar cells and thin film solar cells.<sup>18,19</sup> However, the use of copper sulfide as a CE material in DSSCs has been rarely reported until now. Lam and co-workers reported a copper sulfide-based CE fabricated from precursor decomposition method involving a high temperature (500 °C) sintering process. It showed a 3.79% PCE for the  $\text{I}^-/\text{I}_3^-$  redox system.<sup>20</sup>

In this work,  $\text{Cu}_9\text{S}_5$  nanocrystalline film was fabricated directly onto the FTO substrate by a solution-processed spin-coating technique with a low temperature post-treatment at

<sup>a</sup>State Key Laboratory of Fine Chemicals, Institute of Artificial Photosynthesis, DUT-KTH Joint Education and Research Center on Molecular Devices, Dalian University of Technology (DUT), Dalian 116024, China. E-mail: ze.yu@dlut.edu.cn; symbueno@dlut.edu.cn

<sup>b</sup>Department of Chemistry, School of Chemical Science and Engineering, KTH Royal Institute of Technology, 100 44 Stockholm, Sweden

† Electronic supplementary information (ESI) available. See DOI: 10.1039/c7ra06822k



250 °C and it was further explored as a CE material in DSSCs. The CV and EIS results revealed that Cu<sub>9</sub>S<sub>5</sub> film exhibited a higher electrocatalytic activity for the cobalt-based system relative to the iodine-based electrolyte. Consequently, the DSSC devices based on the cobalt complex redox shuttles showed a PCE of 5.7% at 100 mW cm<sup>-2</sup> illumination (AM 1.5G), which was considerably higher than that of iodine-based electrolyte (3.9%).

## 2. Experimental

### 2.1. Materials

Chemicals and solvents, including *tert*-butanol (96%), 4-*tert*-butylpyridine (TBP, 96%), *li*-bis(trifluoromethanesulfonyl) imide (Li-TFSI), copper chloride (CuCl<sub>2</sub>), thioacetamide (TAA), and *N,N*-dimethylformamide (DMF) were purchased from Sigma-Aldrich. Sensitizer LEG4 was purchased from Dyenamo AB, Sweden. Mesoporous TiO<sub>2</sub> paste and scattering layer TPP200 paste were provided by Heptachroma, China.

### 2.2. Preparation of CEs

FTO conducting glass substrates were washed by detergent, deionized water, and ethanol. Then, the substrates were further treated by UVO-Cleaner for 30 min. The preparation of the precursor solutions as follows:<sup>19</sup> an equiv. of CuCl<sub>2</sub> was dispersed in DMF by ultrasound to dissolve. Then 4 equiv. of TAA was added and stirred for 2 hours until a blood red precursor solution was obtained. The solution was filtered before use. The digenite Cu<sub>9</sub>S<sub>5</sub> CE was prepared by spin-coating of the precursor solution on a freshly cleaned FTO substrate at a speed of 2000 rpm for 30 s. After being sintered at 250 °C on hot plate for 1 min, Cu<sub>9</sub>S<sub>5</sub> counter electrode was obtained.

### 2.3. Fabrication of DSSC devices

The DSSC devices were fabricated as reported previously.<sup>21</sup> The well cleaned FTO substrate was soaked in 40 mM TiCl<sub>4</sub> aqueous solution at 70 °C for 30 min, and then sintered at 500 °C for 30 min to fabricate the compact TiO<sub>2</sub> blocking layer. The mesoporous layer and scattering layer were fabricated *via* screen-printing of TiO<sub>2</sub> 18NR-T paste (three times, every time dried at 130 °C for 5 min) and TPP200 paste, respectively. After sintering (500 °C, 30 min), the films were dipped into TiCl<sub>4</sub> aqueous solution again. The final TiO<sub>2</sub> film was soaked in a LEG4 dye solution (1 × 10<sup>-4</sup> M) in acetonitrile and *tert*-butanol mixed solvent (1 : 1, v/v) overnight. DSSCs with the Cu<sub>9</sub>S<sub>5</sub> counter electrode and the photoanode TiO<sub>2</sub> electrode were assembled using a surlyn film (25 μm) as a spacer. Different electrolytes were injected into interlayer through a pinhole. The symmetrical dummy cells were fabricated by two identical counter electrodes (CE/electrolytes/CE), and the electrolytes were the same as used for the DSSCs devices. The iodine-based electrolyte was the same as previously reported.<sup>21</sup> The iodine-based electrolyte consisted of 0.60 M 1,2-dimethyl-3-propylimidazolium iodide (DMPII), 0.02 M I<sub>2</sub>, 0.06 M LiI, and 0.40 M TBP in acetonitrile. The [Co(bpy)<sub>3</sub>]<sup>2+/3+</sup> electrolyte was

made of 0.22 M [Co(bpy)<sub>3</sub>](PF<sub>6</sub>)<sub>2</sub>, 0.05 M [Co(bpy)<sub>3</sub>](PF<sub>6</sub>)<sub>3</sub>, 0.10 M Li-TFSI, and 0.50 M TBP in acetonitrile.<sup>22</sup>

### 2.4. Characterizations and measurements

XRD was measured with an automatic X-ray powder diffractometer (D/Max 2400, Rigaku, Japan). X-ray photon spectroscopy (XPS, Escalab 250Xi, Thermo Fisher) was implemented to measure the binding energies of digenite Cu<sub>9</sub>S<sub>5</sub> film. The morphology and structure of the Cu<sub>9</sub>S<sub>5</sub> CE was obtained by field-emission scanning electron microscopy (FE-SEM, Nova Nano SEM 450, USA) and atomic force microscopy (AFM, XE-70, Korea). The electrochemical characterizations of Cu<sub>9</sub>S<sub>5</sub> CE were performed by electrochemical workstation (CHI660E, Chenhua, Shanghai). It was conducted using a three-electrode system with as-prepared Cu<sub>9</sub>S<sub>5</sub> film on FTO as a working electrode. Pt wire electrode and Ag/AgNO<sub>3</sub> were used as counter electrode and a reference electrode, respectively. The cobalt complex-based solution is composed of 20 mM [Co(bpy)<sub>3</sub>](PF<sub>6</sub>)<sub>2</sub>, 5 mM [Co(bpy)<sub>3</sub>](PF<sub>6</sub>)<sub>3</sub>, and 100 mM LiClO<sub>4</sub> in acetonitrile. The iodine-based solution contained 10 mM LiI, 1 mM I<sub>2</sub>, and 100 mM LiClO<sub>4</sub> in acetonitrile. The active area of working electrode was controlled at 1 cm<sup>2</sup> and the scan rate was 50 mV s<sup>-1</sup>. EIS was obtained by using a Zennium analyzer system (Model: IM6, Zahner, German) with a frequency range from 10<sup>6</sup> Hz to 0.1 Hz. The photovoltaic performance were determined by photocurrent density–voltage (*J*–*V*) curves and incident photon-to-current conversion efficiency (IPCE) spectra. The test instruments include a Keithley 2400 Source-measure with an Oriel Sol3A solar simulator (Model: 94023A, Newport USA) and Hypermonolight (SM-25, Japan).

## 3. Results and discussion

### 3.1. Composition and morphology

Fig. 1 displays the XRD patterns of Cu<sub>9</sub>S<sub>5</sub> film on FTO (red line) and a bare FTO (black line) for reference. It indicates that Cu<sub>9</sub>S<sub>5</sub> was successfully *in situ* grown on the FTO substrate. A sharp diffraction peak at position 46.2° corresponds to the (0120) plane, indicative of the good crystallization of as-prepared Cu<sub>9</sub>S<sub>5</sub> film. The peaks observed at diffraction angles of 27.8°, 32.3° and 54.9° correspond to the (0015), (1010), (1115) crystal planes, respectively, in a good line with the reported data (JCPD card, no. 47-1748) and previous report.<sup>19</sup> XPS was carried out to further confirm the structure of Cu<sub>9</sub>S<sub>5</sub> film on the FTO substrate. The peaks at binding energy energies of 931.95 and 932.85 eV in Fig. S1a† are attributed to Cu 2P peaks of the Cu<sup>+</sup> and Cu<sup>2+</sup>. The double peaks at about 162 eV in Fig. S1b† correspond to the S 2P peaks of S<sup>2-</sup>. These results agree well with characteristics of Cu<sub>9</sub>S<sub>5</sub> as previously reported.<sup>19</sup>

Fig. 2a and b exhibit the FE-SEM results of Cu<sub>9</sub>S<sub>5</sub> film with different magnifications. A nanoporous network is clearly observed for the as-prepared film. Large specific surface area is expected to deliver more catalytic active sites, and thus enhancing the CE's electrocatalytic ability.<sup>9</sup> Moreover, the nanoporous structure is also beneficial for the diffusion of the electrolytes.<sup>23</sup> The energy-dispersive X-ray spectroscopy (EDS)



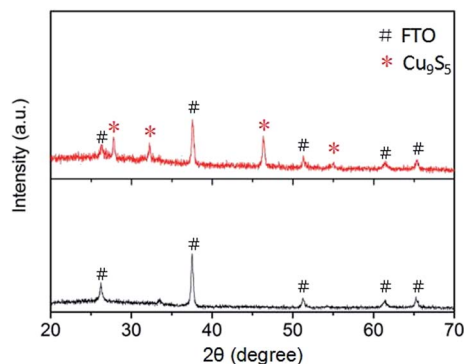


Fig. 1 XRD spectra of  $\text{Cu}_9\text{S}_5$  film on FTO (red line) and bare FTO (black line).

elemental mappings show uniform distributions of elements of Cu and S grown within the film,<sup>24</sup> as presented in Fig. S2.† AFM was performed to evaluate the surface three-dimensional

morphology, as depicted in Fig. 2c. The root-mean-square roughness (RMS) of  $\text{Cu}_9\text{S}_5$  film is 74.47 nm, which is much larger than that of Pt (RMS = 8.82 nm) (Fig. S3†). The result indicates that  $\text{Cu}_9\text{S}_5$  film has unsmooth surface, which is consistent with the SEM images. Here, we conclude that well-crystallized digenite  $\text{Cu}_9\text{S}_5$  film with high surface area was *in situ* grown on the FTO glass through a low-temperature solution-processable method from a simple precursor solution.

### 3.2. Electrochemical properties

To explore the electrocatalytic ability of the  $\text{Cu}_9\text{S}_5$  CE for both the iodine- and cobalt-based redox electrolytes, CV measurement was performed. It was conducted using a three-electrode system with as-prepared  $\text{Cu}_9\text{S}_5$  film on FTO as a working electrode. Pt wire electrode and  $\text{Ag}/\text{AgNO}_3$  were used as counter electrode and a reference electrode, respectively. The cobalt complex-based solution is composed of 20 mM  $[\text{Co}(\text{bpy})_3](\text{PF}_6)_2$ , 5 mM  $[\text{Co}(\text{bpy})_3](\text{PF}_6)_3$ , and 100 mM  $\text{LiClO}_4$  in acetonitrile. The

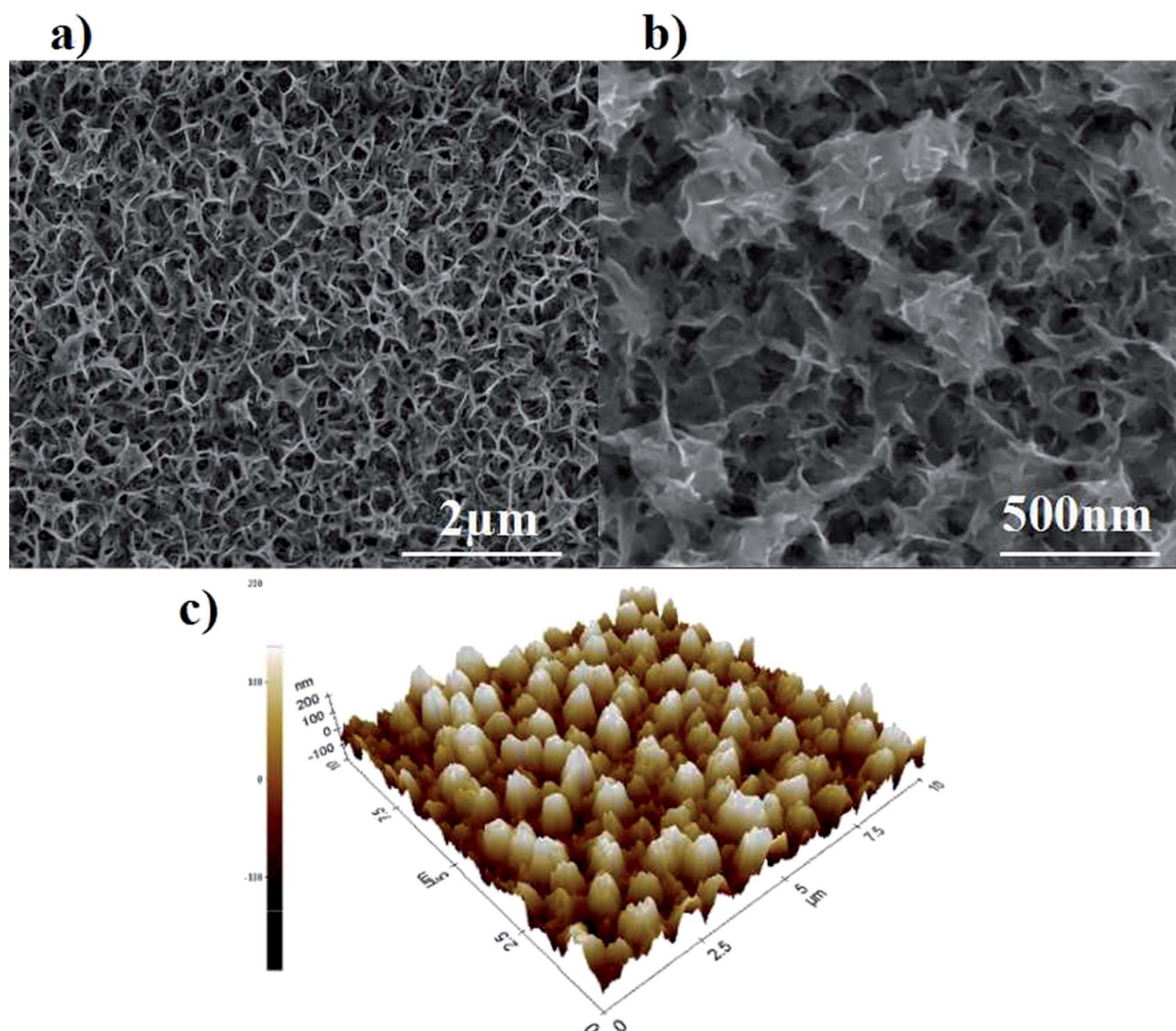


Fig. 2 (a and b) FE-SEM images of  $\text{Cu}_9\text{S}_5$  film on FTO substrate at different magnifications; (c) AFM image of  $\text{Cu}_9\text{S}_5$  film on FTO substrate.





iodine-based solution contained 10 mM LiI, 1 mM I<sub>2</sub>, and 100 mM LiClO<sub>4</sub> in acetonitrile. Generally, the catalytic activities was determined by the peak current density and the peak distance between the oxidation peak and reduction peak ( $E_{pp}$ ).<sup>25</sup> For a CE, large peak current density and small  $E_{pp}$  are two important parameters to determine high electrocatalytic ability of a CE catalyst.<sup>24</sup> Fig. 3a depicts the CV of Cu<sub>9</sub>S<sub>5</sub> electrode in cobalt complex-based electrolyte. A redox event is clearly observed in the CV curve (Fig. 3a), which is assigned to the redox reaction of  $\text{Co}^{3+} + \text{e}^- \leftrightarrow \text{Co}^{2+}$ . In DSSCs, the dye cations are regenerated by  $\text{Co}^{2+}$  cations, which are oxidized to  $\text{Co}^{3+}$  cations afterwards. The resulting  $\text{Co}^{3+}$  cations are reduced back to  $\text{Co}^{2+}$  cations at CE/electrolyte interface. Consequently, the reduction peak should be the research emphasis for the CV study.<sup>26</sup> In the CV curve, Cu<sub>9</sub>S<sub>5</sub> electrode exhibits a high reduction peak current density ( $J_{RE}$ ) of 0.85 mA cm<sup>-2</sup> and an  $E_{pp}$  of 272 mV, which are close to the corresponding value obtained for Pt electrode ( $J_{RE}$  1.0 mA cm<sup>-2</sup>,  $E_{pp}$  219 mV) (Fig. S4†). This result indicates that the Cu<sub>9</sub>S<sub>5</sub> film is expected to have comparable catalytic activity for the reduction of  $\text{Co}^{3+}$  cations complex relative to Pt. The high surface of the nanoporous Cu<sub>9</sub>S<sub>5</sub>

electrode most likely provides a more reduction sites, thus enhancing catalytic ability. It is also worth mentioning that the  $J_{RE}$  of Cu<sub>9</sub>S<sub>5</sub> CE remained almost unchanged after 50 cycles as shown in Fig. S4,† indicating the good electrochemical stability of Cu<sub>9</sub>S<sub>5</sub> electrode for the reduction of cobalt(III) species. The electrocatalytic ability of the Cu<sub>9</sub>S<sub>5</sub> CE for the iodine-based electrolyte was also studied and the CV curve is depicted in Fig. 3b. By stark contrast, for the iodine-based redox couple, the Cu<sub>9</sub>S<sub>5</sub> CE exhibited two pairs of irreversible redox peaks. In particular, the weak cathodic peak at the left part of the CV curve is attributed to the reduction of the I<sub>3</sub><sup>-</sup> ions ( $\text{I}_3^- + 2\text{e}^- \rightarrow 3\text{I}^-$ ). This result implies the poor electrocatalytic activity of Cu<sub>9</sub>S<sub>5</sub> electrode towards the reduction of I<sub>3</sub><sup>-</sup> ions.

EIS measurements were performed with an aim to further examine the electrocatalytic property of Cu<sub>9</sub>S<sub>5</sub> electrode in different electrolytes by using a dummy cell with two identical electrodes (CE/Electrolyte/CE). Fig. 4a presents the Nyquist plots of the [Co(bpy)<sub>3</sub>]<sup>2+/3+</sup> and I<sup>-</sup>/I<sub>3</sub><sup>-</sup> redox electrolytes measured at a bias voltage of 0.3 V under dark condition. The equivalent circuit model is presented in the inset. For a better comparison, the enlarged part of the Nyquist plots is also given

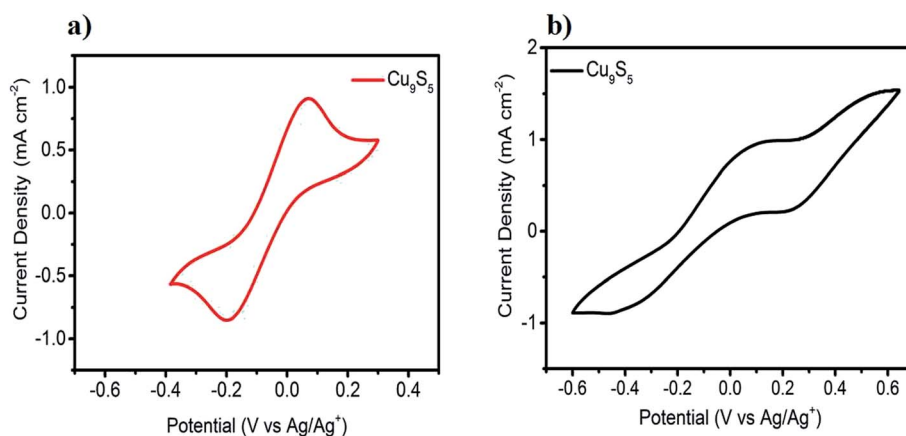


Fig. 3 Cyclic voltammograms for prepared Cu<sub>9</sub>S<sub>5</sub> electrode: (a) cobalt complex-based electrolyte in acetonitrile solution of 20 mM [Co(bpy)<sub>3</sub>](PF<sub>6</sub>)<sub>2</sub>, 5 mM [Co(bpy)<sub>3</sub>](PF<sub>6</sub>)<sub>3</sub>, and 100 mM LiClO<sub>4</sub>; (b) iodine-based electrolyte in acetonitrile solution of 10 mM LiI, 1 mM I<sub>2</sub>, and 100 mM LiClO<sub>4</sub>.

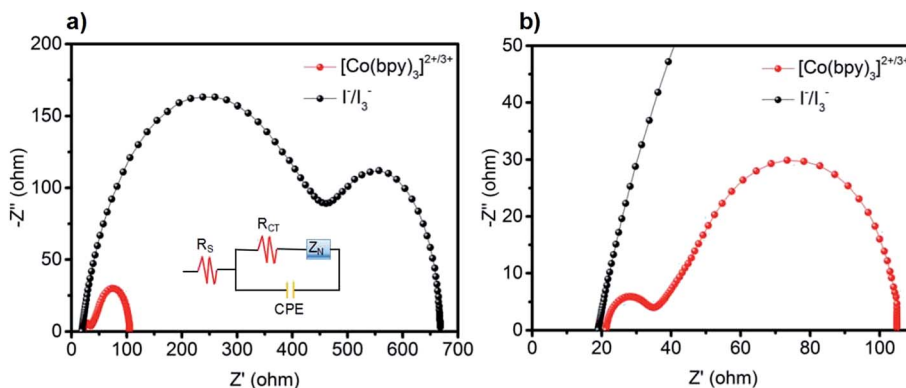


Fig. 4 (a) Nyquist plots of the prepared Cu<sub>9</sub>S<sub>5</sub> electrode in a dummy cell with [Co(bpy)<sub>3</sub>]<sup>2+/3+</sup> and I<sup>-</sup>/I<sub>3</sub><sup>-</sup> based electrolytes, the inset is the equivalent circuit used to model the impedance spectra; (b) enlarged Nyquist plots of (a).



(Fig. 4b). Two semicircles can be observed for these two redox systems. The high-frequency one corresponds to the charge-transfer resistance ( $R_{CT}$ ) at the CE/electrolyte interface. The semicircle observed in the low-frequency range reflects the Nernst diffusion impedance ( $Z_N$ ) of the redox couples in the electrolyte.<sup>16</sup> The  $R_{CT}$  of the cobalt-based redox couple is estimated to be 12.3  $\Omega$ , which is significantly lower than that of  $I^-/I_3^-$  (422  $\Omega$ ). The smaller  $R_{CT}$  further indicates that  $Cu_9S_5$  electrode shows good electrocatalytic ability towards the reduction of  $Co^{3+}$  species, which is in a good line with the CV curves. The EIS of Pt CE under the same conditions were also tested for comparison as presented in Fig. S5.† For the cobalt-based system, the  $R_{CT}$  value of Pt CE is estimated to be 7.2  $\Omega$ , which is slightly smaller relative to  $Cu_9S_5$  based CE. Here, it emphasizes again that  $Cu_9S_5$  CE has good electrocatalytic activity towards the reduction of the  $Co^{3+}$  species, which can rival the state-of-the-art Pt electrode. To further study the electrocatalytic activities of  $Cu_9S_5$  CE for different electrolytes, Tafel polarization curves were conducted using symmetric cell as in EIS. Fig. S6† shows the Tafel polarization curves of the  $Cu_9S_5$  electrode with different electrolytes in the potential range from  $-0.6$  to  $+0.6$  V. For the iodine-based electrolyte, the plot is not a normal smooth line and the exchange current density is much lower than that of cobalt-based electrolyte. These results further verifies that  $Cu_9S_5$  film is not a suitable catalytic material for the  $I^-/I_3^-$  redox system. Overall, from the CV, EIS and Tafel results, we infer that the  $Cu_9S_5$  CE would be a potential counter electrode for cobalt complex-based electrolytes in DSSCs.

### 3.3. Photovoltaic performance of DSSCs

We further examined photovoltaic performance of  $Cu_9S_5$  CEs in DSSCs using cobalt complex- and iodine-based redox electrolytes. The photocurrent density–voltage ( $J$ - $V$ ) characteristics of the best solar cells measured at 100  $mW\ cm^{-2}$  illumination AM 1.5G (active area 0.16  $cm^2$ ) are displayed in Fig. 5a and the corresponding parameters are summarized in Table 1. The DSSC device based on  $[Co(bpy)_3]^{2+/3+}$  system exhibited an open-circuit voltage ( $V_{oc}$ ) of 0.78 V, a short-circuit

**Table 1** Photovoltaic parameters of DSSCs based on  $Cu_9S_5$  counter electrode using  $[Co(bpy)_3]^{2+/3+}$  and  $I^-/I_3^-$  based electrolytes measured under AM 1.5G simulated sunlight (100  $mW\ cm^{-2}$ )

Redox couples	$V_{oc}$ (V)	$J_{sc}$ ( $mA\ cm^{-2}$ )	$FF$	$PCE$ (%)
$[Co(bpy)_3]^{2+/3+}$	0.78	13.7	0.53	5.7
$I^-/I_3^-$	0.69	12.3	0.46	3.9

current density ( $J_{sc}$ ) of 13.7  $mA\ cm^{-2}$ , and a fill factor ( $FF$ ) of 0.53, giving a PCE of 5.7%. By comparison, all the photovoltaic parameters for the  $I^-/I_3^-$  system are lower than the corresponding values of the cobalt complex counterpart. DSSC device used  $I^-/I_3^-$  electrolyte showed a much lower PCE of only 3.9%, with a  $V_{oc}$  of 0.69 V, a  $J_{sc}$  of 12.3  $mA\ cm^{-2}$ , and a  $FF$  of 0.46. Strikingly, the cobalt-based electrolyte displayed a comparatively higher  $FF$  (0.53) as compared to the  $I^-/I_3^-$  redox system (0.46). This should be attributed to a significantly lower  $R_{CT}$  observed for the cobalt-based redox couple as confirmed by the EIS measurements discussed above. Generally,  $V_{oc}$  is mainly governed by the potential gap between the Fermi energy level of the  $TiO_2$  and the redox potential of the redox mediator in the electrolyte. From the previous report, the redox potential of  $[Co(bpy)_3]^{2+/3+}$  is 0.56 V vs. NHE, while the corresponding value of the  $I^-/I_3^-$  is 0.35 V vs. NHE.<sup>21</sup> Thus, the difference for the  $V_{oc}$  values observed should be mainly attributed to more positive redox potential of the cobalt complexes. Fig. 5b shows the IPCE spectra of DSSCs based on these two redox electrolytes. The trend of IPCE measurements is in good agreement with  $J_{sc}$  obtained from  $J$ - $V$  characterizations. The photovoltaic performance of Pt CE, as a reference, was also tested for the  $[Co(bpy)_3]^{2+/3+}$  based electrolyte under identical conditions (Fig. S7†). The solar cell based on Pt CE exhibited a PCE of 8.5% with an improved  $FF$  (0.67). The different performances of Pt and  $Cu_9S_5$  CEs most likely lies in the fact that  $Cu_9S_5$  CE has a low intrinsic conductivity and thus a larger charge transfer resistance.

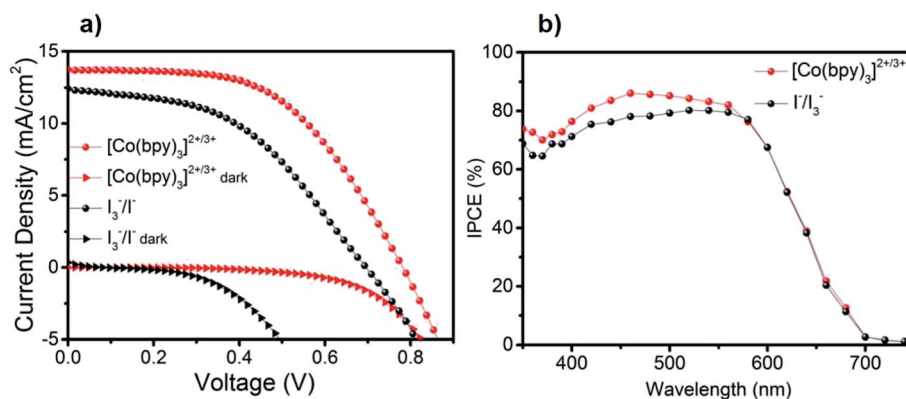


**Fig. 5** (a) Photocurrent density–voltage ( $J$ - $V$ ) curves of DSSCs using  $Cu_9S_5$  CE with  $[Co(bpy)_3]^{2+/3+}$  and  $I^-/I_3^-$  based electrolytes measured under AM 1.5G simulated sunlight (100  $mW\ cm^{-2}$ ) and in dark condition; (b) the incident photon-to-current conversion efficiency (IPCE) spectra of DSSCs using  $Cu_9S_5$  CE with  $[Co(bpy)_3]^{2+/3+}$  and  $I^-/I_3^-$  based electrolytes.



## 4. Conclusions

In conclusion, we developed a  $\text{Cu}_9\text{S}_5$  nanocrystalline film, which was fabricated directly onto the FTO substrate by a low temperature solution-processed method, as a low-cost CE material in DSSCs. The results from CV and EIS measurements demonstrated that  $\text{Cu}_9\text{S}_5$  film displayed a higher electrocatalytic ability for the state-of-the-art  $[\text{Co}(\text{bpy})_3]^{2+/3+}$  redox system in comparison to the widely used iodine-based electrolyte. Consequently, DSSC devices incorporating cobalt complex redox shuttles showed a considerably higher PCE, which is attributed mainly to the low  $R_{\text{CT}}$  at the CE/electrolyte interface and good catalytic ability of  $\text{Cu}_9\text{S}_5$  electrode towards reduction of the cobalt(III) species. There is still a potential room for further enhancement of the efficiency of  $\text{Cu}_9\text{S}_5$  CE. One possible strategy would be to couple it with highly conductive carbon materials, as demonstrated by several successful examples reported previously.<sup>24,27</sup> Nevertheless, the present work will shed interesting light on identifying alternative low-cost and efficient CE materials, in particular for non-iodine based electrolytes in DSSCs in the future.

## Acknowledgements

We acknowledge the financial support from the National Natural Science Foundation of China (21606039, 21673028, 51661135021, 91233201), the Fundamental Research Funds for the Central Universities, Swedish Foundation for Strategic Research (SSF), the Swedish Energy Agency, as well as the Knut and Alice Wallenberg Foundation.

## References

- 1 B. O'regan and M. Grätzel, *Nature*, 1991, **353**, 737–740.
- 2 S. M. Feldt, E. A. Gibson, E. Gabrielsson, L. Sun, G. Boschloo and A. Hagfeldt, *J. Am. Chem. Soc.*, 2010, **132**, 16714–16724.
- 3 A. Yella, H. W. Lee, H. N. Tsao, C. Yi, A. K. Chandiran, M. K. Nazeeruddin, E. W.-G. Diau, C.-Y. Yeh, S. M. Zakeeruddin and M. Grätzel, *Science*, 2011, **334**, 629–633.
- 4 S. Mathew, A. Yella, P. Gao, R. Humphry-Baker, B. F. E. Curchod, N. Ashari-Astani, I. Tavernelli, U. Rothlisberger, M. K. Nazeeruddin and M. Grätzel, *Nat. Chem.*, 2014, **6**, 242–247.
- 5 M. Wu and T. Ma, *J. Phys. Chem. C*, 2014, **118**, 16727–16742.
- 6 M. Wu, X. Lin, T. Wang, J. Qiu and T. Ma, *Energy Environ. Sci.*, 2011, **4**, 2308–2315.
- 7 H. N. Tsao, J. Burschka, C. Yi, F. Kessler, M. K. Nazeeruddin and M. Grätzel, *Energy Environ. Sci.*, 2011, **4**, 4921–4924.
- 8 J. Briscoe and S. Dunn, *Adv. Mater.*, 2016, **28**, 3802–3813.
- 9 M. Wang, A. Anghel, B. Marsan, N. Ha, N. Pootrakulchote, S. Zakeeruddin and M. Grätzel, *J. Am. Chem. Soc.*, 2009, **131**, 15976–15977.
- 10 C. Kung, H. Chen, C. Lin, K. Huang, R. Vittal and K. Ho, *ACS Nano*, 2012, **6**, 7016–7025.
- 11 H. Sun, D. Qin, S. Huang, X. Guo, D. Li, Y. Luo and Q. Meng, *Energy Environ. Sci.*, 2011, **4**, 2630–2637.
- 12 D. Y. Wang, Y. T. Jiang, C. C. Lin, S. S. Li, Y. T. Wang, C. C. Chen and C. W. Chen, *Adv. Mater.*, 2012, **24**, 3415–3420.
- 13 Y. C. Wang, D. Y. Wang, Y. T. Jiang, H. A. Chen, C. C. Chen, K. C. Ho, H. L. Chou and C. W. Chen, *Angew. Chem., Int. Ed.*, 2013, **52**, 6694–6698.
- 14 Y. Wang, S. Li, Y. Bai, Z. Chen, Q. Jiang, T. Li and W. Zhang, *Electrochim. Acta*, 2013, **114**, 30–34.
- 15 E. Singh, K. S. Kim, G. Y. Yeom and H. S. Nalwa, *ACS Appl. Mater. Interfaces*, 2017, **9**, 3223–3245.
- 16 N. Huang, G. Li, Z. Xia, F. Zheng, H. Huang, W. Li, C. Xiang, Y. Sun, P. Sun and X. Sun, *Electrochim. Acta*, 2017, **235**, 182–190.
- 17 S. Infant Raj, X. Xu, W. Yang, F. Yang, L. Hou and Y. Li, *Electrochim. Acta*, 2016, **212**, 614–620.
- 18 M. Venkata-Haritha, C. V. V. M. Gopi, Y. S. Lee and H. J. Kim, *RSC Adv.*, 2016, **6**, 101185–101197.
- 19 M. J. Zhang, Q. Lin, X. Yang, Z. Mei, J. Liang, Y. Lin and F. Pan, *Nano Lett.*, 2016, **16**, 1218–1223.
- 20 H. K. Mulmudi, S. K. Batabyal, M. Rao, R. R. Prabhakar, N. Mathews, Y. M. Lam and S. G. Mhaisalkar, *Phys. Chem. Chem. Phys.*, 2011, **13**, 19307–19309.
- 21 J. Li, X. Yang, Z. Yu, G. G. Gurzadyan, M. Cheng, F. Zhang, J. Cong, W. Wang, H. Wang, X. Li, L. Kloo, M. Wang and L. Sun, *RSC Adv.*, 2017, **7**, 4611–4615.
- 22 H. N. Tsao, C. Yi, T. Moehl, J. H. Yum, S. M. Zakeeruddin, M. K. Nazeeruddin and M. Grätzel, *ChemSusChem*, 2011, **4**, 591–594.
- 23 M. Wu, X. Lin, Y. Wang, L. Wang, W. Guo, D. Qi, X. Peng, A. Hagfeldt, M. Grätzel and T. Ma, *J. Am. Chem. Soc.*, 2012, **134**, 3419–3428.
- 24 Z. Xie, X. Cui, W. Xu and Y. Wang, *Electrochim. Acta*, 2017, **229**, 361–370.
- 25 H. Li, Y. Xiao, G. Han and W. Hou, *J. Power Sources*, 2017, **342**, 709–716.
- 26 X. Yin, F. Wu, N. Fu, J. Han, D. Chen, P. Xu, M. He and Y. Lin, *ACS Appl. Mater. Interfaces*, 2013, **5**, 8423–8429.
- 27 M. Guo, F. Zhao, Y. Yao, S. Wang and S. Yin, *Electrochim. Acta*, 2016, **205**, 15–19.

